

Article

Fabrication of a Potential Electrodeposited Nanocomposite for Dental Applications

Chun-Wei Chang ^{1,†}, Chen-Han Tsou ^{2,†}, Bai-Hung Huang ^{3,4}, Kuo-Sheng Hung ^{5,6}, Yung-Chieh Cho ⁷, Takashi Saito ⁸, Chi-Hsun Tsai ⁸, Chia-Chien Hsieh ⁹, Chung-Ming Liu ^{3,*} and Wen-Chien Lan ^{10,*}

¹ Division of Endodontics, Department of Dentistry, Taipei Medical University Hospital, Taipei 110, Taiwan

² Department of Dentistry, Zuoying Branch of Kaohsiung Armed Forces General Hospital, Kaohsiung 813, Taiwan

³ Department of Biomedical Engineering, College of Biomedical Engineering, China Medical University, Taichung 404, Taiwan

⁴ Graduate Institute of Dental Science, College of Dentistry, China Medical University, Taichung 404, Taiwan

⁵ Graduate Institute of Injury Prevention and Control, College of Public Health, Taipei Medical University, Taipei 110, Taiwan

⁶ Department of Neurosurgery, Taipei Medical University-Wan Fang Hospital, Taipei, Taipei 116, Taiwan

⁷ School of Dentistry, College of Oral Medicine, Taipei Medical University, Taipei 110, Taiwan

⁸ Division of Clinical Cariology and Endodontology, Department of Oral Rehabilitation, School of Dentistry, Health Sciences University of Hokkaido, Hokkaido 061-0293, Japan

⁹ Graduate Institute of Biomedical Optomechatronics, College of Biomedical Engineering, Taipei Medical University, Taipei 110, Taiwan

¹⁰ Department of Oral Hygiene Care, Ching Kuo Institute of Management and Health, Keelung 203, Taiwan

* Correspondence: liuc@mail.cmu.edu.tw (C.-M.L.); jameslan@ems.cmu.edu.tw (W.-C.L.)

† These authors contributed equally to this work.



Citation: Chang, C.-W.; Tsou, C.-H.; Huang, B.-H.; Hung, K.-S.; Cho, Y.-C.; Saito, T.; Tsai, C.-H.; Hsieh, C.-C.; Liu, C.-M.; Lan, W.-C. Fabrication of a Potential Electrodeposited Nanocomposite for Dental Applications. *Inorganics* **2022**, *10*, 165. <https://doi.org/10.3390/inorganics10100165>

Academic Editor: Roberto Nisticò

Received: 12 July 2022

Accepted: 15 September 2022

Published: 3 October 2022

Publisher's Note: MDPI stays neutral with regard to jurisdictional claims in published maps and institutional affiliations.



Copyright: © 2022 by the authors. Licensee MDPI, Basel, Switzerland. This article is an open access article distributed under the terms and conditions of the Creative Commons Attribution (CC BY) license (<https://creativecommons.org/licenses/by/4.0/>).

Abstract: In the present study, a nanocrystalline Ni-Fe matrix with reinforced TiO₂ nanoparticles as a functional nanocomposite material was fabricated by pulsed current electroforming in UV-LIGA (lithography, electroplating, and molding). The influences of TiO₂ nanoparticles on the Ni-Fe nanocomposite deposition were also investigated using scanning electron microscopy, transmission electron microscopy, and in vitro cytotoxicity assay. It was found that the Ni-Fe nanocomposite with 5 wt.% TiO₂ nanoparticles showed a smooth surface and better dispersion property. When the Ni-Fe nanocomposite is combined with 20 wt.% TiO₂, it resulted in congeries of TiO₂ nanoparticles. In addition, TiO₂ nanoparticles possessed better dispersion properties as performed in pulse current electrodeposition. The microstructure of the electrodeposited Ni-Fe-TiO₂ nanocomposite was a FeNi₃ phase containing anatase nano-TiO₂. Moreover, the electrodeposited Ni-Fe-5 wt.% TiO₂ nanocomposite exhibited a smooth surface and structural integrity. Cytotoxicity assay results also proved that the Ni-Fe nanocomposite with different concentrations of TiO₂ nanoparticles had good biocompatibility. Therefore, the optimization of pulse current electroforming parameters was successfully applied to fabricate the Ni-Fe-TiO₂ nanocomposite, and thus could be used as an endodontic file material for dental applications.

Keywords: Ni-Fe-TiO₂ nanocomposite; microstructure; biocompatibility; endodontic file

1. Introduction

Nickel-based alloys have been extensively used as endodontic files for root canal treatment in dental fields because of their unique advantages such as high strength and toughness, superior flexibility, good shape-memory ability, excellent corrosion resistance, and acceptable biocompatibility [1–5]. Despite the advantages of nickel-based alloys, nickel-based endodontic files fracture caused by torsional and cyclic fatigue in root canal treatment still is the main issue in clinical applications [6–8]. It is well known that metallic material with a nanocrystalline structure improves mechanical properties [9–12]. Accordingly, it

would be desirable if the traditional nickel-based alloy could be developed as a nanocomposite with high torsional and cyclic fatigue resistance using potential fabrication methods or by adding reinforced nanostructured materials to avoid fracture formation in root canal without sacrificing desirable physicochemical and biological properties.

There are extensive studies on methods to produce nanocrystalline materials such as current electroplating, electroless plating, co-deposition processes, pulse plating, etc. [9,12–18]. In general, electrodeposition produced porosity-free products and no consolidation was required. In contrast, nanocrystalline precursor powders were considered a vital raw material in other processing methods. Many pure metals such as Pd, Co, Ni, Ni–Mo Ni–Zn, Ni–Fe, binary alloys, and Ni–Fe–Cr ternary alloys have been fabricated by the above-mentioned methods [19–24]. Electrodeposition can produce nanostructured materials with selected treatment parameters such as pH value, overpotential, bath composition, temperature, etc. [25–27], while electrocrystallization occurs through two competing processes (existing crystals buildup and new materials formation) and can be affected by several factors. The ratio of the two processes was determined by the diffusion status of anions on the surface of crystal and charge transfer rate on the surface of the electrode [28]. Low over potential and high surface diffusion rates could cause grain growth, while high over potential and low diffusion rates of surface promote the new nuclei formation. The current density allowed by pulse plating is much higher than the limited direct current density, which can improve the new nuclei formation [29]. As stated above, the goal of the present study aimed to fabricate the Ni-Fe with reinforced Ti dioxide (Ni-Fe-TiO₂) nanocomposite (nanocrystalline Ni-Fe matrix and TiO₂ nanoparticles) as a potential endodontic instrument by the co-deposition approach with pulse electroplating for dental applications. Properties of the Ni-Fe-TiO₂ nanocomposites were evaluated through material analyses and biocompatibility assays.

2. Results

2.1. Electrodeposition of the Ni-Fe-TiO₂ Nanocomposites

According to the used parameters of pulse plating, it was found that the deposited nanocomposites exhibited extremely shiny and smooth surface features. Moreover, the TiO₂ concentration of the samples changed from 0.1 ± 0.1 wt.% (minimum) to a concentration of 2.9 ± 0.1 wt.% (maximum) for the plating solution. Different parameters such as TiO₂ concentration in the plating solution, duty cycle, current density, and solution agitation affected the TiO₂ concentration in the electrodeposits. The TiO₂ concentration in the plating solution was affected most at peak current density. Enhancing the TiO₂ concentration of the solution could increase the TiO₂ amount in the electrodeposition. However, the amount of electrodeposited TiO₂ reduced as the peak current density increased.

2.2. Microstructural Characterization of the Ni-Fe-TiO₂ Nanocomposites

The microstructure of the Ni-Fe-5 wt.% TiO₂ nanocomposite is shown in Figure 1. The formation of a nanocrystalline Ni-Fe matrix with irregularly shaped TiO₂ particles (as indicated by black arrows) can be clearly seen. The TiO₂ particles were evenly dispersed in the Ni-Fe matrix. Chemical compositions of the Ni-Fe-5 wt.% TiO₂ nanocomposite are illustrated in Figure 2. Based on the analysis by EDS, only the presence of Ni, Fe, Ti, and O elements can be seen in the matrix. No other contaminants or impurity substances were formed in the matrix during the electrodeposition. Similar microstructural characteristics and chemical compositions could also be found in the other two nanocomposites. The average size of grain in the Ni-Fe matrix was measured using the Scherrer method [11]. It was found that the average size of the grain is between 15 nm~20 nm. One thing to consider during the analysis is that the Scherrer method used in this study might not provide accurate grain sizes because of some effects; for example, the presence of stacking faults and broadening of the diffracted beam caused by microstrains. Thus, TEM was also employed to determine the grain size for the investigated nanocomposites. Figure 3 shows the microstructures and grain sizes of the as-deposited Ni-Fe-5 wt.%

TiO₂. Grain size is calculated from a plan-view of TEM micrograph. Apparently, the as-deposited Ni-Fe matrix was a polycrystalline structure with a grain size of ~50 nm (Figure 3a). The Ni-Fe matrix belongs to the FeNi₃ phase with a face-centered cubic crystalline structure. Moreover, a diffraction ring pattern (Figure 3a) and numerous white nanocrystalline structures (Figure 3b) were seen in the matrix indicating that the TiO₂ nanoparticles were successfully deposited in the nanocomposite matrix. According to the camera length and *d*-spacings from the selected-area diffraction pattern, the deposited TiO₂ belongs to the anatase with a tetragonal crystalline structure. Hence, the microstructure of the electrodeposited Ni-Fe-5 wt.% TiO₂ nanocomposite was FeNi₃ phase containing anatase nano-TiO₂. These features were also discovered in the Ni-Fe-10 wt.% TiO₂ and Ni-Fe-20 wt.% TiO₂ nanocomposites. Figures 4 and 5 present a car-like shape model fabricated with Ni-Fe-5 wt.% TiO₂ nanocomposite through an optimal UV-LIGA method. Clearly, the micro-scale car-like shape model with a smooth surface and structural integrity could be fabricated via this potential method.

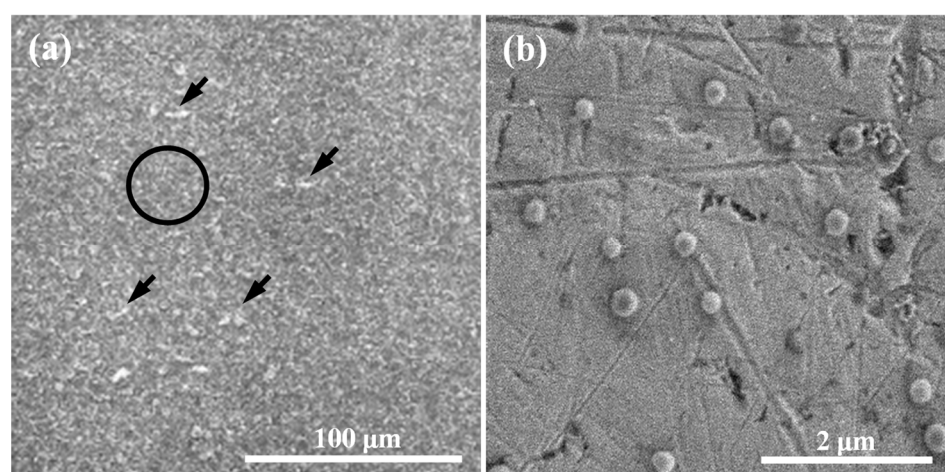


Figure 1. The FE-SEM micrographs of the Ni-Fe-5 wt.% TiO₂ nanocomposite: (a) irregular shaped TiO₂ particles are embedded in a nanocrystalline Ni-Fe matrix and (b) a higher magnification image taken from the Ni-Fe matrix (marked as the black circular area) in (a).

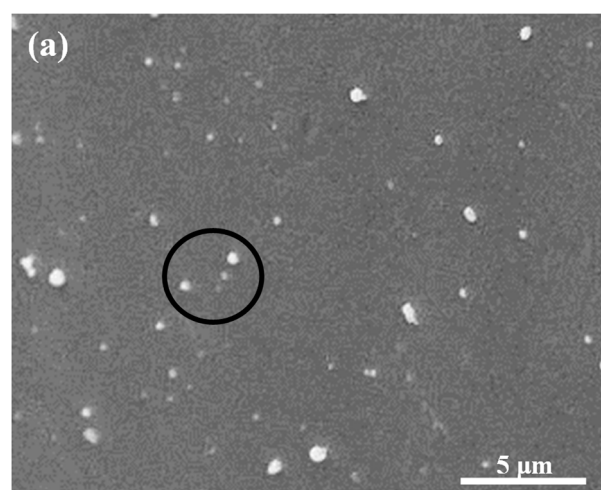


Figure 2. Cont.

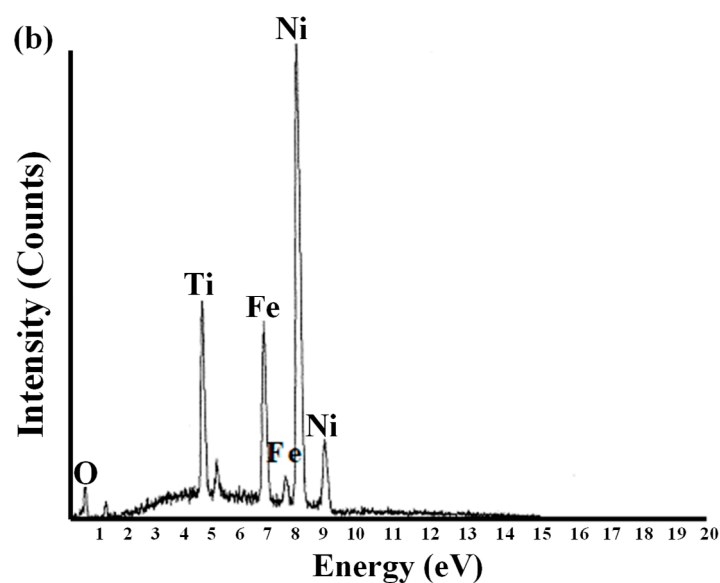


Figure 2. The chemical compositions of the Ni-Fe-5 wt.%TiO₂ nanocomposite: (a) a higher magnification FE-SEM micrograph for EDS analysis and (b) an EDS spectrum taken from the matrix with TiO₂ particles (marked as the black circular area) in (a).

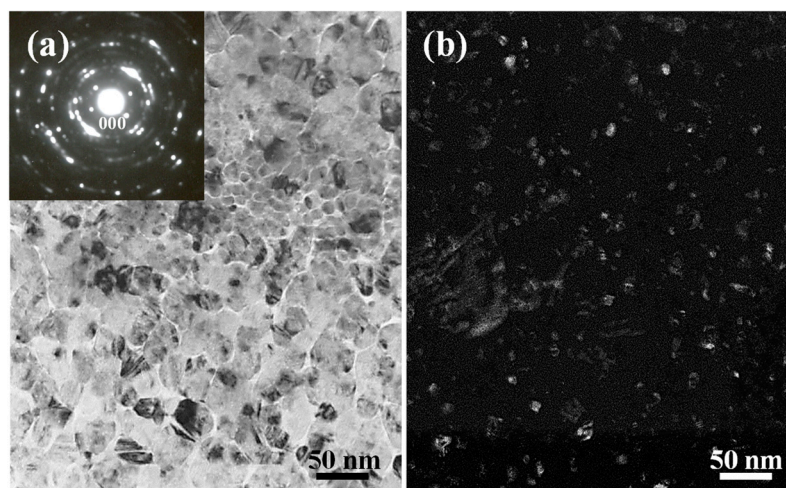


Figure 3. The TEM micrographs of the Ni-Fe-5 wt.%TiO₂ nanocomposite: (a) bright-field image showing the polycrystalline structure in the Ni-Fe matrix and (b) dark-field image indicating the TiO₂ nanocrystallization formation.

2.3. Cell Viability and Adhesion Behavior of the Ni-Fe-TiO₂ Nanocomposites

The cell viability of L929 of the Ni-Fe-TiO₂ nanocomposites for 24 h is shown in Figure 6a. Obviously, the Ni-Fe-TiO₂ nanocomposites exhibited a cell survival rate of more than 70%. It is considered an acute cytotoxic potential when the cell viability of the sample is less than <70% of the blank, according to ISO 10993-5. No statistically significant difference ($n = 5$) between investigated Ni-Fe-TiO₂ nanocomposites. Following cell seeding on the Ni-Fe-TiO₂ nanocomposites, morphology and cell adhesion in Ni-Fe-TiO₂ nanocomposites were observed through FE-SEM as illustrated in Figure 6b. It was found that all Ni-Fe-TiO₂ nanocomposites showed numerous elongated filopodia after 3 days of cell seeding. The filopodia of cells not only adhered flat, but also tightly grabbed the surface structure (as indicated by arrows). The cell viability and response features demonstrated all Ni-Fe-TiO₂ nanocomposites possessed good biocompatibility.

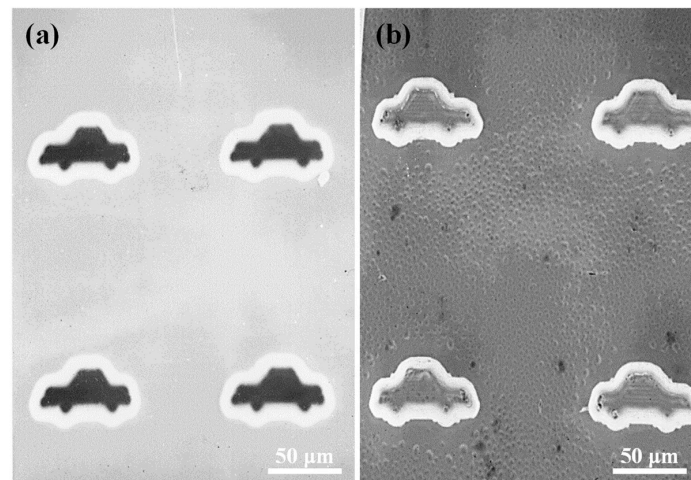


Figure 4. The FE-SEM micrographs of a car-like shape model of the Ni-Fe-5 wt.% TiO₂ nanocomposite fabricated through an optimal UV-LIGA method: (a) car-like cavity image and (b) car-like shape image.

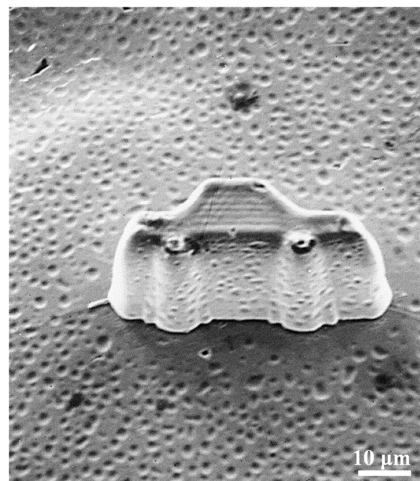


Figure 5. A higher magnification FE-SEM micrograph of the car-like shape model. The electrodeposited micro-scale car-like shape model exhibits a smooth surface and structural integrity.

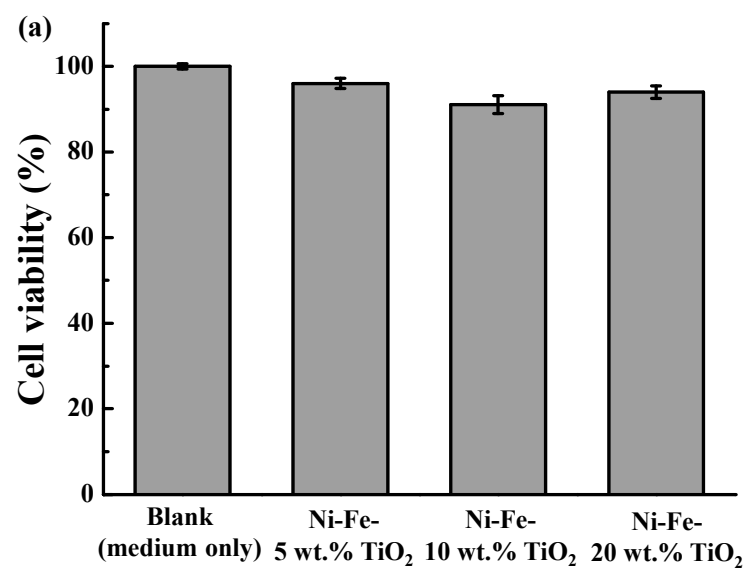


Figure 6. *Cont.*

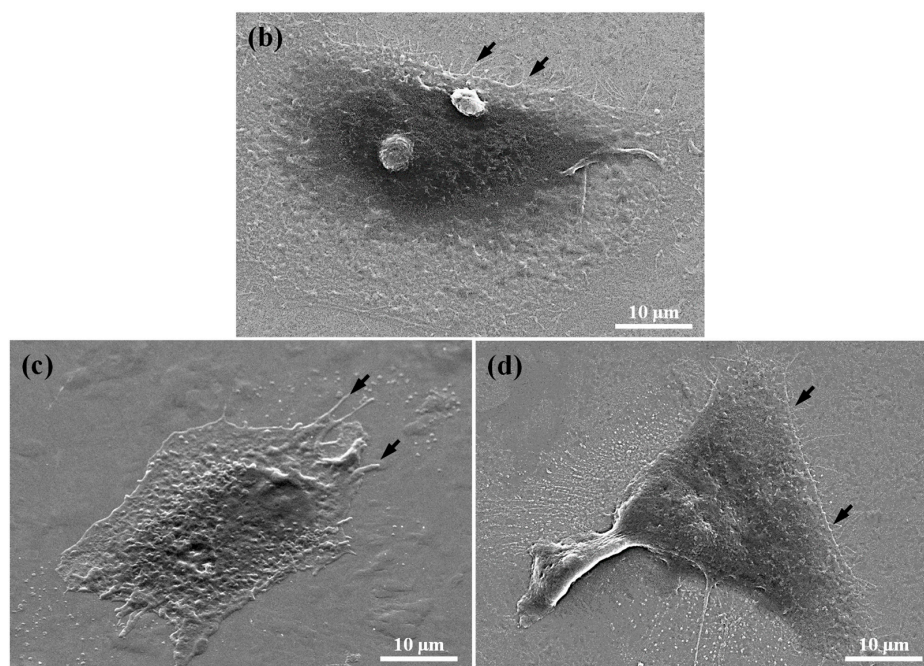


Figure 6. (a) Cell viability of L929 of the Ni-Fe-TiO₂ nanocomposites for 24 h and cell morphologies of the Ni-Fe-TiO₂ nanocomposites after culturing with L929 cells for 3 days: (b) Ni-Fe-5 wt.% TiO₂, (c) Ni-Fe-10 wt.% TiO₂, and (d) Ni-Fe-20 wt.% TiO₂. The filopodia (as indicated by arrows) of cells not only adhered flat, but also tightly grabbed the surface structure.

3. Discussion

In this study, it was found that the electrodeposited nanocomposite produced better smooth sidewall and surface as well as structural integrity, revealing that the Ni-Fe alloy with TiO₂ nanoparticles promoted formability. To explore possible reinforcement factors in nanocomposite materials, we compared results from different groups of nanocomposites including a traditional matrix of polycrystalline Ni containing reinforced nanoparticles of Al₂O₃ [30]. Oberle et al. [31] reported that with large hardness and mechanical strength enhancement in the composite matrix, the volume fraction of the co-deposited oxide reinforcements with 50 nm and 300 nm particle sizes is relatively low (i.e., 1–2% volume). Muller et al. [32] also indicated that there was a hardness and mechanical strength increased in the co-deposited Ni nanocomposite matrix containing at least 23 vol.% of Al₂O₃ (average 14 nm in diameter), and grain size of Ni is over 50 nm. However, the fabricated Ni-Fe with reinforced TiO₂ nanoparticles nanocomposite exhibited a similar microstructure texture with a grain size of ~50 nm. The grain size decreased when TiO₂ nanoparticles were added, which indicated that the nanocrystallization effect would occur due to the reactions of energetic ions in the solution during electrodeposition [22,33].

For a small matrix, the grain size was only meaningful within a limited range when used in nanocrystalline range dislocation models. The concept of the original dislocation model of the Hall-Petch relationship was based on that grain boundaries were played as barriers to dislocation movement, so a pile-up of dislocation formed at grain boundaries. As the length of pile-up with a range of 10–100 nm, the models of pile-up become doubtful. For example, the nanocrystalline range of dislocations in a pile-up rapidly reduced when the size of the grain decreased [34]. Likewise, the typical mechanism of the Orowan type was unlikely to work in the investigated nanocomposite material, since the particles of reinforcing were one order of magnitude larger than the average grain size of the matrix at least, leading to a structure in which one hard particle was surrounded by numerous differently oriented grains in the matrix of Ni-Fe. Accordingly, the nanocomposite materials with higher mechanical strength were mainly owing to the nanocrystalline Ni matrix with

the presence of a reinforced second phase [35]. It is believed that the mechanical properties can be promoted for the Ni-Fe-TiO₂ nanocomposite.

Cytotoxicity testing is designed to assess the general toxicity of biomaterials and medical devices. The test consists of extracting the device in a cell culture medium and then exposing the extract to L929 mouse fibroblasts. ISO 10993-5 specification indicates reasonable cell viability of 70% under the MTT assay. Cell viability near or below 70% may be highly toxic to cells. In the present study, cell viability results showed that the investigated Ni-Fe-TiO₂ nanocomposites had high cell viability of over 90% after culturing with L929 cells for 24 h. A high cell viability rate reveals that the investigated material possesses better cell proliferation behavior and excellent biocompatibility [36,37]. In addition, it was found that there was no statistically significant difference between investigated Ni-Fe-TiO₂ nanocomposites. These findings demonstrated the electrodeposited Ni-Fe-TiO₂ nanocomposites with different concentrations of TiO₂ nanoparticles did not influence the proliferation and adhesion behaviors of L929 cells. Nanostructured TiO₂ has broad potential applications due to its nanosized features, low toxicity, and good biocompatibility [38]. Mohammadi et al. [39] also indicated that the mechanical strength of calcium phosphate cement can be enhanced with TiO₂ nanoparticles addition in the short-term. As a result, it is believed that the electrodeposited Ni-Fe-TiO₂ nanocomposites can not only enhance cell viability but can also improve mechanical properties to obtain the desired results. As discussed above, the optimal Ni-Fe-TiO₂ nanocomposite can be fabricated through the UV-LIGA approach. The Ni-Fe-TiO₂ is a potential nanocomposite material that could be unitized as an endodontic file for dental applications. However, further studies should be performed to provide additional information concerning the mechanical properties including micro-hardness, tensile strength, torsional strength, and cyclic fatigue in the presence of electrodeposited Ni-Fe-TiO₂ nanocomposites.

4. Materials and Methods

4.1. Materials Preparation

In this study, a modified Watts bath solution [40] was adopted as a plating solution and TiO₂ nanoparticles with an average diameter of 40 nm (Merk Taiwan, Taipei, Taiwan) were used as reinforced material. The pH value was controlled at a range of 2.5–3.5. Ni carbonate and hydrochloric/sulphuric acid (ratio 1:9) were used for pH value adjustment. Before fabrication, the TiO₂ nanoparticles powder was slowly added to the modified Watts bath solution with continuous mixing to avoid the TiO₂ nanoparticles agglomeration. Subsequently, the TiO₂ slurry with different concentrations of 5 wt.%, 15 wt.%, and 20 wt.% was added to the solution of bulk in the final bath, respectively. Hereafter, the pulsed electrodeposition process was performed with a galvanostat/potentiostat electrochemical instrument (EG & G, Princeton Applied Research 263A, Artisan Technology Group, Champaign, IL, USA), which could control the direct or pulsed electrodepositions. The parameter of pulse plating of duty cycle (pulse on time divided by pulse on time plus pulse off time) was set in direct current between 30% and 100%. The peak current densities were up to 10 A/dm². The stirring rate was calculated by means of a mechanical impeller to maintain the TiO₂ particulate in suspension. The time of plating was set constantly at 750 rpm for 3 h. The plating solution contained in the plating cell was kept in a water bath at 60 °C. The plating cell anode was made by the electrolytic Ni (purity 99.99%) containing Ti basket. The cathode was made by the Ti substrate (1 cm × 2 cm). Finally, the electrodeposits were mechanically removed from the Ti substrate (cathode side) to analyze surface and microstructural characterizations.

4.2. Surface Characterization

Surface morphology was studied by a JEOL JSM-6500F field emission scanning electron microscope (FE-SEM, Tokyo, Japan) equipped with a high-energy dispersive X-ray spectroscope (EDS; INCA, Oxford Instruments, Abingdon, UK). The operating voltage was kept at 20 kV. The samples were observed and analyzed under different magnifications.

4.3. Microstructure Identification

The model 657 dimple grinder (Gatan Inc., Pleasanton, CA, USA) and model 691 precision ion polishing system (Gatan Inc., Pleasanton, CA, USA) were used to prepare the TEM specimen with an electron transparent area. Hereafter, a model JEOL-2100 high-resolution transmission electron microscope (TEM; JEOL Ltd., Tokyo, Japan) was used to research crystallinity and phase identification with an accelerating voltage of 200 kV.

4.4. Cytotoxicity Assay

In this study, the L929 RM60091 mouse fibroblast cell line (Bioresource Collection, and Research Center, Hsinchu, Taiwan) was used for cytotoxicity evaluation. The cells were seeded in culture dishes at a density of 5×10^4 cells per 100 μL in α -Minimum Essential Medium (MEM; Level Biotechnology, New Taipei City, Taiwan). Cells from passage 2 were harvested at 80% confluence and used for further 3-(4,5-dimethylthiazol-2-yl)-2,5-diphenyltetrazolium bromide (MTT) assay. The extracts of the investigated samples were placed in an orbital shaker maintained at 37 °C for 24 h with a mass to volume extraction ratio of 0.2 g/mL, which was followed by filtering and sealing in sterile bottles. L929 cells at a density of 1×10^4 cells/well were cultured in MEM and seeded on the 24-well culture plates. After obtaining a confluent monolayer, the medium was replaced by 0.1 mL sample extracts and incubated for 24 h at 37 °C in an atmosphere of 5% CO_2 ($n = 5$). Afterward, a 10 μL MTT assay kit (R&D system, Minneapolis, MN, USA) was added to each well and incubated for 2 h. The optical density value of each plate was read at 570 nm through the ELx800 microplate reader (BioTek, Winooski, VT, USA). According to ISO 10993-5 specification, the cell viability (%) in the short-term culturing (24 h) experiment was adopted to assess the material's acute cytotoxicity response.

4.5. Cell Morphology Observation

The morphology of L929 cells was observed after 3 days of culture. The adhered L929 cells were washed with PBS, placed in a fixative consisting of 2.5% glutaraldehyde in 0.1 M sodium cacodylate buffer for 1 h at 4 °C, rinsed in deionized water, and dehydrated in serial of ethanol solutions for 15 min each concentration. Hereafter, dehydrated samples were soaked in hexamethyldisilazane, sputter coated with platinum, and analyzed with JEOL-6500F FE-SEM at 25 kV under different magnifications.

4.6. Statistical Analysis

The experimental results with multiple readings are presented as mean \pm standard deviation. Data were analyzed through the variance from the Student's *t*-test (Excel 2016 version, Microsoft Corporation, Redmond, WA, USA). *P* values ≤ 0.05 were considered statistically significant.

5. Conclusions

The present work fabricated a potential nanocomposite material consisting of anatase TiO_2 nanoparticles contained in the nanocrystalline matrix of Ni-Fe using electrodeposition from a modified Watts bath. The size of grain in the nanocrystalline Ni-Fe matrix decreased with the addition of the TiO_2 nanoparticles. The Ni-Fe- TiO_2 nanocomposite exhibited a smooth surface and structural integrity. The TiO_2 nanoparticles doped in the Ni-Fe alloy can facilitate formability. The electrodeposited Ni-Fe- TiO_2 nanocomposites with different concentrations of TiO_2 nanoparticles did not influence the proliferation and adhesion behaviors of cells. Therefore, the electrodeposited Ni-Fe- TiO_2 nanocomposite is a promising endodontic file material for dental applications.

Author Contributions: Writing—original draft, C.-W.C.; Investigation, C.-W.C. and C.-H.T. (Chen-Han Tsou); Data curation, C.-C.H. and C.-H.T. (Chi-Hsun Tsai); Methodology, B.-H.H.; Supervision, T.S.; Resources, Y.-C.C.; Validation, K.-S.H.; Writing—review & editing, W.-C.L. and C.-M.L. All authors have read and agreed to the published version of the manuscript.

Funding: The authors would like to thank the Zuoying Branch of Kaohsiung Armed Forces General Hospital and Taipei Medical University Hospital for financially supporting this research under contract no. KAFGH-ZY-A-110015 and 111-D-TMUH-003.

Institutional Review Board Statement: Not applicable.

Informed Consent Statement: Not applicable.

Data Availability Statement: Data is contained within the article.

Conflicts of Interest: The authors declare no conflict of interest.

References

1. Bhagyashree, B.; Rao, D.; Panwar, S.; Kothari, N.; Gupta, S. An in vitro comparative evaluation of dentinal crack formation caused by three different nickel-titanium rotary file systems in primary anterior teeth. *J. Indian Soc. Pedod. Prev. Dent.* **2022**, *40*, 188–194.
2. Dhaimy, S.; Kim, H.C.; Bedida, L.; Benkiran, I. Efficacy of reciprocating and rotary retreatment nickel-titanium file systems for removing filling materials with a complementary cleaning method in oval canals. *Restor. Dent. Endod.* **2021**, *46*, e13. [[CrossRef](#)] [[PubMed](#)]
3. Hasheminia, S.M.; Farhad, A.; Davoudi, H.; Sarfaraz, D. Microleakage of five separated nickel-titanium rotary file systems in the apical portion of the root canal. *Dent. Res. J.* **2022**, *19*, 46.
4. Huang, Z.; Quan, J.; Liu, J.; Zhang, W.; Zhang, X.; Hu, X. A microcomputed tomography evaluation of the shaping ability of three thermally-treated nickel-titanium rotary file systems in curved canals. *J. Int. Med. Res.* **2019**, *47*, 325–334. [[CrossRef](#)]
5. Tabassum, S.; Zafar, K.; Umer, F. Nickel-titanium rotary file systems: What's new? *Eur. Endod. J.* **2019**, *4*, 111–117.
6. Ruiz-Sanchez, C.; Faus-Llacer, V.; Faus-Matoses, I.; Zubizarreta-Macho, A.; Sauro, S.; Faus-Matoses, V. The influence of niti alloy on the cyclic fatigue resistance of endodontic files. *J. Clin. Med.* **2020**, *9*, 3755. [[CrossRef](#)] [[PubMed](#)]
7. Machado, R.; Junior, C.S.; Colombelli, M.F.; Picolli, A.P.; Junior, J.S.; Cosme-Silva, L.; Garcia, L.; Alberton, L.R. Incidence of protaper universal system instrument fractures—A retrospective clinical study. *Eur. Endod. J.* **2018**, *3*, 77–81. [[CrossRef](#)] [[PubMed](#)]
8. Patnana, A.K.; Chugh, A.; Chugh, V.K.; Kumar, P. The incidence of nickel-titanium endodontic hand file fractures: A 7-year retrospective study in a tertiary care hospital. *J. Conserv. Dent.* **2020**, *23*, 21–25. [[CrossRef](#)]
9. Han, Q.G.; Zhang, H.Z.; Fang, L.; Wang, Y.Q. Tribological properties of nanocrystalline cu coatings produced by electroless plating under various lubrication conditions. *Rare Met. Mater. Eng.* **2011**, *40*, 356–359.
10. Gorka, J.; Czuprynski, A.; Zuk, M.; Adamiak, M.; Kopysc, A. Properties and structure of deposited nanocrystalline coatings in relation to selected construction materials resistant to abrasive wear. *Materials* **2018**, *11*, 1184. [[CrossRef](#)]
11. Matsui, I.; Mori, H.; Kawakatsu, T.; Takigawa, Y.; Uesugi, T.; Higashi, K. Mechanical behavior of electrodeposited bulk nanocrystalline fe-ni alloys. *Mater. Res. Ibero Am. J.* **2015**, *18*, 95–100. [[CrossRef](#)]
12. Latha, N.; Raj, V.; Selvam, M. Effect of plating time on growth of nanocrystalline ni-p from sulphate/glycine bath by electroless deposition method. *Bull. Mater. Sci.* **2013**, *36*, 719–727. [[CrossRef](#)]
13. Byun, M.H.; Cho, J.W.; Han, B.S.; Kim, Y.K.; Song, Y.S. Material characterization of electroplated-nanocrystalline nickel-iron alloys for micro electronic mechanical-system. *Jpn. J. Appl. Phys.* **2006**, *45*, 7084–7090. [[CrossRef](#)]
14. See, S.H.; Seet, H.L.; Li, X.P.; Lee, J.Y.; Lee, K.Y.T.; Teoh, S.H.; Lim, C.T. Effect of nanocrystalline electroplating of nife on the material permeability. *Mater. Sci. Forum* **2003**, *437–438*, 53–56. [[CrossRef](#)]
15. Hu, J.J.; Chai, L.J.; Xu, H.B.; Ma, C.P.; Deng, S.B. Microstructural modification of brush-plated nanocrystalline cr by high current pulsed electron beam irradiation. *J. Nano Res. Sw.* **2016**, *41*, 87–95. [[CrossRef](#)]
16. Kosta, I.; Vincenzo, A.; Muller, C.; Sarret, M. Mixed amorphous-nanocrystalline cobalt phosphorous by pulse plating. *Surf. Coat. Tech.* **2012**, *207*, 443–449. [[CrossRef](#)]
17. Protsenko, V.S.; Danilov, F.I.; Gordiienko, V.O.; Baskevich, A.S.; Artemchuk, V.V. Improving hardness and tribological characteristics of nanocrystalline cr-c films obtained from cr(iii) plating bath using pulsed electrodeposition. *Int. J. Refract. Met. Hard Mater.* **2012**, *31*, 281–283. [[CrossRef](#)]
18. Zhang, H.Z.; Fang, L.; Zhou, Y.G.; Shi, G.L. Microstructures and corrosion properties of nanocrystalline cu coatings synthesized by electroless plating. *Rare Met. Mater. Eng.* **2012**, *41*, 239–242.
19. Dmitriev, A.I.; Nikonov, A.Y.; Osterle, W. Molecular dynamics sliding simulations of amorphous ni, ni-p and nanocrystalline ni films. *Comp. Mater. Sci.* **2017**, *129*, 231–238. [[CrossRef](#)]
20. Tsyntsaru, N.; Kaziukaitis, G.; Yang, C.; Cesiulis, H.; Philipsen, H.G.G.; Lelis, M.; Celis, J.P. Co-w nanocrystalline electrodeposits as barrier for interconnects. *J. Solid State Electr.* **2014**, *18*, 3057–3064. [[CrossRef](#)]
21. Umopathy, G.; Senguttuvan, G.; Berchmans, L.J.; Sivakumar, V.; Jegatheesan, P. Influence of cerium substitution on structural, magnetic and dielectric properties of nanocrystalline ni-zn ferrites synthesized by combustion method. *J. Mater. Sci. Mater. El.* **2017**, *28*, 17505–17515. [[CrossRef](#)]
22. Farshbaf, P.A.; Bostani, B.; Yaghoobi, M.; Farshbaf, P.A.; Bostani, B.; Yaghoobi, M.; Ahmadi, N.P. Evaluation of corrosion resistance of electrodeposited nanocrystalline ni-fe alloy coatings. *Trans. Inst. Met. Finish.* **2017**, *95*, 269–275. [[CrossRef](#)]
23. Bigos, A.; Beltowska-Lehman, E.; Kot, M. Studies on electrochemical deposition and physicochemical properties of nanocrystalline ni-mo alloys. *Surf. Coat. Tech.* **2017**, *317*, 103–109. [[CrossRef](#)]

24. Wang, C.S.; Su, H.J.; Guo, Y.A.; Guo, J.T.; Zhou, L.Z. Solidification characteristics and segregation behavior of a ni-fe-cr based alloy. *Rare Met. Mat. Eng.* **2018**, *47*, 3816–3823. [[CrossRef](#)]
25. Sharma, A.; Bhattacharya, S.; Das, S.; Das, K. A study on the effect of pulse electrodeposition parameters on the morphology of pure tin coatings. *Met. Mater. Trans. A* **2014**, *45*, 4610–4622. [[CrossRef](#)]
26. Kolonits, T.; Czigany, Z.; Peter, L.; Bakonyi, I.; Gubicza, J. Influence of bath additives on the thermal stability of the nanostructure and hardness of ni films processed by electrodeposition. *Coatings* **2019**, *9*, 644. [[CrossRef](#)]
27. Torabinejad, V.; Aliofkhaeaei, M.; Assareh, S.; Allahyarzadeh, M.H.; Rouhaghdam, A.S. Electrodeposition of ni-fe alloys, composites, and nano coatings—a review. *J. Alloy. Compd.* **2017**, *691*, 841–859. [[CrossRef](#)]
28. Tripkovic, D.V.; Strmcnik, D.; van der Vliet, D.; Stamenkovic, V.; Markovic, N.M. The role of anions in surface electrochemistry. *Faraday Discuss.* **2008**, *140*, 25–40. [[CrossRef](#)]
29. Sun, J.; Du, D.X.; Lv, H.F.; Zhou, L.; Wang, Y.G.; Qi, C.G. Microstructure and corrosion resistance of pulse electrodeposited ni-cr coatings. *Surf. Eng.* **2015**, *31*, 406–411. [[CrossRef](#)]
30. Muller, B.; Ferkel, H. Properties of nanocrystalline ni/al₂o₃ composites. *Z. Metallkd.* **1999**, *90*, 868–871.
31. Oberle, R.R.; Scanlon, M.R.; Cammarata, R.C.; Searson, P.C. Processing and hardness of electrodeposited ni/al₂o₃ nanocomposites. *Appl. Phys. Lett.* **1995**, *66*, 19–21. [[CrossRef](#)]
32. Muller, B.; Ferkel, H. Al₂o₃-nanoparticle distribution in plated nickel composite films. *Nanostructured Mater.* **1998**, *10*, 1285–1288. [[CrossRef](#)]
33. Nicolenco, A.; Mulone, A.; Imaz, N.; Tsyntaru, N.; Sort, J.; Pellicer, E.; Klement, U.; Cesiulis, H.; Garcia-Lecina, E. Nanocrystalline electrodeposited fe-w/al₂o₃ composites: Effect of alumina sub-microparticles on the mechanical, tribological, and corrosion properties. *Front. Chem.* **2019**, *7*, 241. [[CrossRef](#)] [[PubMed](#)]
34. Arzt, E. Overview no. 130—Size effects in materials due to microstructural and dimensional constraints: A comparative review. *Acta Mater.* **1998**, *46*, 5611–5626. [[CrossRef](#)]
35. Zimmerman, A.F.; Clark, D.G.; Aust, K.T.; Erb, U. Pulse electrodeposition of ni-sic nanocomposite. *Mater. Lett.* **2002**, *52*, 85–90. [[CrossRef](#)]
36. Hsu, H.J.; Abd Waris, R.; Ruslin, M.; Lin, Y.H.; Chen, C.S.; Ou, K.L. An innovative alpha-calcium sulfate hemihydrate bioceramic as a potential bone graft substitute. *J. Am. Ceram. Soc.* **2018**, *101*, 419–427. [[CrossRef](#)]
37. Gittens, R.A.; McLachlan, T.; Olivares-Navarrete, R.; Cai, Y.; Berner, S.; Tannenbaum, R.; Schwartz, Z.; Sandhage, K.H.; Boyan, B.D. The effects of combined micron-/submicron-scale surface roughness and nanoscale features on cell proliferation and differentiation. *Biomaterials* **2011**, *32*, 3395–3403. [[CrossRef](#)]
38. Jafari, S.; Mahyad, B.; Hashemzadeh, H.; Janfaza, S.; Gholikhani, T.; Tayebi, L. Biomedical applications of tio₂ nanostructures: Recent advances. *Int. J. Nanomed.* **2020**, *15*, 3447–3470. [[CrossRef](#)]
39. Mohammadi, M.; Hesarakhi, S.; Hafezi-Ardakani, M. Investigation of biocompatible nanosized materials for development of strong calcium phosphate bone cement: Comparison of nano-titania, nano-silicon carbide and amorphous nano-silica. *Ceram. Int.* **2014**, *40*, 8377–8387. [[CrossRef](#)]
40. Ibrahim, M.A.M. Black nickel electrodeposition from a modified watts bath. *J. Appl. Electrochem.* **2006**, *36*, 295–301. [[CrossRef](#)]